Check for updates

Effects of the cross-linked structures of polymer gels containing iron porphyrins on photoreduction of carbon dioxide†

Shota Furusawa, Masanori Nagao, [iD] * Hikaru Matsumoto [iD] and Yoshiko Miura [iD] *

We prepared polystyrene-based polymer gels containing iron porphyrin and evaluated the effects of the cross-linked structures on the photoreduction of carbon dioxide to carbon monoxide. The amount of generated carbon monoxide was influenced by the diffusion of the substrates into the gel structures.

As industrial development progresses, the concentration of CO_2 emissions in the atmosphere continues to rise, thereby contradicting efforts toward carbon neutrality.[1] This has led to a growing focus on utilizing CO_2 as a raw material for C1 compounds like CH_4,[2,3] CH_3OH,[4,5] and $HCOOH$,[6,7] as well as for petrochemicals. Utilizing CO_2 in this way could help address the urgent challenges of global warming and fossil fuel depletion simultaneously.[8] However, obtaining these raw materials directly from CO_2 is challenging, so they are typically used in reactions after being converted to CO through reduction process involving two-electrons.[9,10] While electrochemical reduction is effective for CO_2 reduction,[11–13] photochemical reduction plays a crucial role in advancing toward a carbon-neutral society by harnessing cleaner energy sources like sunlight (visible light).[14,15]

Metal porphyrins with transition metals (*e.g.*, Fe, Co and Ni) have been used for CO_2 photoreduction.[15–18] Metal porphyrins can store and supply many electrons to the metal site, making it possible to achieve two-electron reduction of CO_2.[19] Many studies have been focusing on catalyst design in homogeneous systems. Aukauloo and co-workers designed iron-coordinated tetraphenyl porphyrin (FeTPP) catalysts with urea functional groups as scaffolds for multi-point hydrogen bonding to CO_2.[20] Furthermore, heterogeneous systems using metal porphyrins as constituent units, such as metal organic frameworks,[17,21,22] covalent organic frameworks,[23–25] and hydrogen-bonded organic framework[26] have been reported.

The use of heterogeneous catalysts enables easy recovery of the catalysts from reaction solution, which encourages their practical applications.[27]

Polymers are used as supports for immobilized catalysts due to their ease of preparation, achieved by polymerizing the catalytic functional group as a monomer.[28–32] However, heterogeneous reactions with immobilized catalysts often exhibit lower efficiency compared to homogeneous reactions due to the reduced frequency of collisions between the catalysts and substrates. To address this challenge, our group has previously focused on the polymer gel structures. The polymer gels supporting the catalysts have demonstrated excellent substrate diffusion into the cross-linked polymer structures, leading to high reaction efficiency.[32–34] However, to the best of our knowledge, the influence of the polymer structures as heterogeneous catalysts on the CO_2 photoreduction remains unclear.

Herein, we synthesized polystyrene-based polymer gels incorporating FeTPP catalyst and evaluated the effects of cross-linked structures on CO_2 photoreduction (Fig. 1). To introduce the catalyst porphyrin into the polymer structures, a porphyrin monomer with two vinyl groups was synthesized (**TPP-M**, Fig. S1†). The synthesis was conducted using a Rothemund
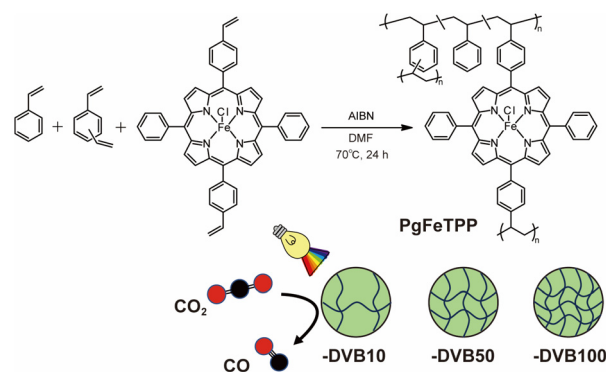
Department of Chemical Engineering, Kyushu University, 744 Motooka, Nishi-ku, Fukuoka 819-0395, Japan. E-mail: nagaom@chem-eng.kyushu-u.ac.jp

Fig. 1 Schematic illustration of the preparation of polymer gels containing FeTPP with different cross-linking ratios.

synthesis approach with 5-phenyldipyrromethane and benz-aldehyde. Subsequently, iron porphyrin monomer (**FeTPP-M**) was obtained through coordination with iron chloride at a high temperature of 120 °C. Porphyrin derivatives exhibit characteristic absorbance peaks within the visible light range in UV-vis spectrum. Following the coordination reaction, the absorbance peaks at Q-bands shifted, indicating successful iron coordination into the porphyrin rings (Fig. S2†).

Polymer gels incorporating FeTPP (**PgFeTPP**) was obtained by copolymerizing styrene, divinylbenzene (DVB, cross-linker), and **FeTPP-M**. Three types of **PgFeTPP** were prepared by varying the amount of DVB, resulting in ratios of DVB to total monomer weight were 10, 50 and 100 wt% (Table 1, **PgFeTPP-DVB10**, **PgFeTPP-DVB50**, and **PgFeTPP-DVB100**, respectively). In addition, a polymer gel without porphyrin (**Pg**) and that containing **TPP-M** (**PgTPP**) were also prepared for comparison (Table 1). After washing the polymer gels, the weighed yields were over 80% for all polymer gels. To confirm the gel structures of the synthesized polymers, swollen bulks of **PgFeTPP** series in DMF were cut into 10 mm squares (Fig. 2a–c). These **PgFeTPP** cubes were then immersed sequentially in THF and MeOH to exchange the solvent inside the polymer cubes. After drying MeOH *in vacuo*, the length of one side of the cubes measured 6, 7, and 9 mm for **PgFeTPP-DVB10**, **-DVB50**, and **-DVB100**, respectively (Fig. 2d–f). To further demonstrate the effect of cross-linking ratios on the gel structures, compression test was conducted using **PgFeTPP** series swollen with DMF. In Fig. 3, the maximum strain values indicate the rates of height changes of the polymer gels until they were broken by the compression. The maximum strain values decreased with the cross-linking ratios, indicating that the higher cross-linking ratio rendered the polymer gels more rigid. These demonstrated that the prepared **PgFeTPP** series exhibited swelling with organic solvents, which is a typical feature of polymer gels, and that higher cross-linking ratios resulted in reduced swelling ratios.

For each characterization, the polymer gels were crushed in a dry state using a mortar. The colours of the polymer powders were white, dark purple, and green for **Pg**, **PgTPP**, and **PgFeTPP**, respectively (Fig. S3†). In FT-IR spectra, the characteristic peaks of polystyrene were shown at 695–750 cm^{-1} (Fig. S4†). However, there is no significant difference among the polymer gels because the feed ratio of the porphyrin monomers was small (1 wt%). Absorbance spectra of these polymer powders were
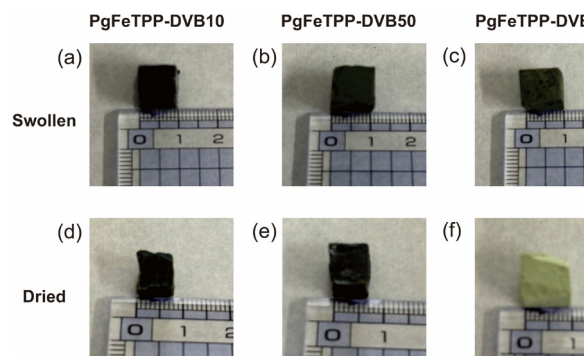

Fig. 2 Photo images of synthesized polymers with distinct cross-linker ratios. (a), (b), and (c) represent the swollen states of **PgFeTPP-DVB10**, **PgFeTPP-DVB50**, and **PgFeTPP-DVB100** with *N*,*N*-dimethylformamide, respectively. (d), (e), and (f) represent the dried states of **PgFeTPP-DVB10**, **PgFeTPP-DVB50**, and **PgFeTPP-DVB100**, respectively.
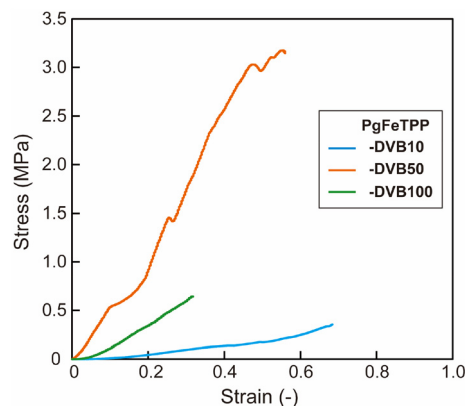

Fig. 3 Stress–strain curves for DMF-swollen **PgFeTPP** series under uni-axial compression. Blue, orange, and green lines represent **PgFeTPP** with DVB contents of 10, 50, and 100 wt%, respectively.

obtained through diffuse reflectance UV–vis measurements. While the polystyrene-based polymer (**Pg**) did not exhibit any absorbance peak in the range from 400 to 800 nm, the polymer containing TPP (**PgTPP**) showed characteristic absorption peaks in the Soret-band (422 nm) and Q-band (519, 551, 599, and 655 nm, Fig. 4a). Furthermore, these peak-top wavelengths were

Table 1 Properties of synthesized polystyrene-based polymer gels

| Entry | Monomer feed ratio (wt%) | | | | Shrinking ratio (vol%)[a] |
	Styrene	DVB	TPP-M	FeTPP-M	
Pg	90	10	—	—	—
PgTPP	89	10	1	—	—
PgFeTPP-DVB10	89	10	—	1	22
PgFeTPP-DVB50	49	50	—	1	34
PgFeTPP-DVB100	—	99	—	1	73

[a] Shrinking ratio was calculated following formula: shrinking ratio (vol%) = 100 × Volume (dried state)/Volume (swollen state).

© 2024 The Author(s). Published by the Royal Society of Chemistry

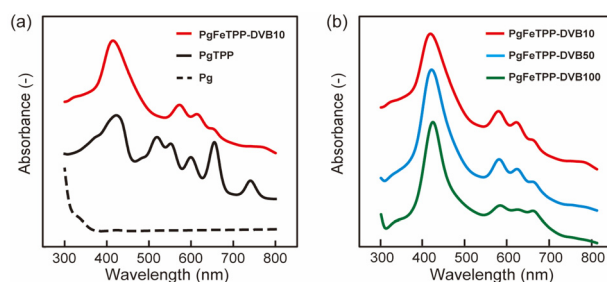*RSC Appl. Polym.*, 2024, **2**, 1026–1031 | **1027**

Fig. 4 Diffuse reflectance UV-vis spectra for polymer powders. (a) **PgFeTPP-DVB10** (red line), **PgTPP** (black line), and **Pg** (dashed line). (b) **PgFeTPP-DVB10** (red line), **PgFeTPP-DVB50** (blue), and **PgFeTPP-DVB100** (green line).

consistent with those of **TPP-M** (Fig. S5a†), demonstrating the incorporation of TPP units into **PgTPP** while maintaining the porphyrin ring structure. A distinct peak at 750 nm observed in the **PgTPP** spectrum was also derived from **TPP-M** (Fig. 4a and S5a†). In diffuse reflectance UV–vis measurements, peaks in the longer wavelength range appear more pronounced due to light scattering. Although the peak at 750 nm was minimal in TPP monomer, the particle morphology of **PgTPP** enhanced the light scattering, thereby making the peak at longer wavelength more prominent. The polymer containing FeTPP (**PgFeTPP-DVB10**) exhibited absorption peaks of the Soret-band (415 nm) and Q-band (572 and 613 nm), which were distinct from those of **PgTPP** (Fig. 4a). The absorbance spectra of **PgFeTPP-DVB10**, **-DVB50**, and **-DVB100** showed the same peak-top wavelengths (Fig. 4b). This suggested that porphyrin rings in **PgFeTPP** had distinct features from those in **PgTPP**. However, diffuse reflectance UV-vis measurements of **FeTPP-M** showed peak-top wavelengths in the Soret band (428 nm) and Q band (514, 569, 658 and 693 nm), which did not match the spectrum of **PgFeTPP** (Fig. S5b†). Considering that the peak-top wavelengths of the **PgTPP** spectrum were consistent with those of **TPP-M** (Fig. S5a†), a possible reason for the lack of match in **PgFeTPP** is the reaction of radical species generated during radical polymerization with the coordinated iron atoms, changing its valence. Next, we evaluated the amount of iron atoms in **PgFeTPP** polymers through X-ray fluorescence measurement. The powders of **PgFeTPP** showed weight fraction of iron atoms over 0.05 wt%, which values were more than 10 times larger than those of **Pg** and **PgTPP** (Fig. 5). This result supports the presence of iron atoms derived from FeTPP within the **PgFeTPP** series. The characterization through UV-vis measurement and XRF analysis indicates the successful preparation of three types of polystyrene-based polymer gels with different cross-linking ratios. Importantly, iron porphyrins were incorporated into these polymers even without a perfect match of chemical structures to its monomer (**FeTPP-M**).

The obtained polymer powders were classified using sieves to minimize the influence of particle size distribution in photoreduction experiments. The particle sizes were categorized as ~53 μm, 53–100 μm, 100–150 μm and 150–200 μm, respectively. Scanning electron microscope (SEM) images of
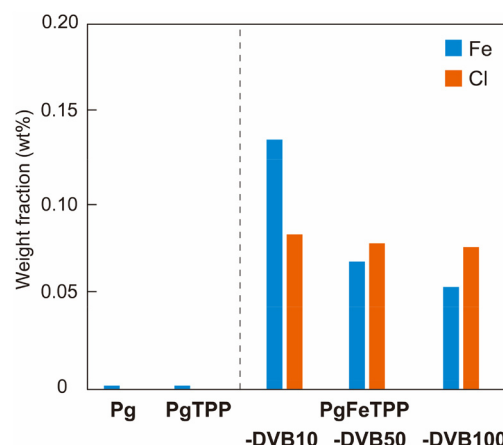

Fig. 5 Weight fraction of Fe and Cl in polymer powders measured by X-ray fluorescence analysis. Blue and orange bars indicate Fe and Cl, respectively.

the particles confirmed the accuracy of the particle size classification by the sieves (Fig. 6).

Photoreduction of CO_2 was performed by irradiating a CO_2-saturated solution of DMF/PhOH (DMF : PhOH = 9.4 mL : 0.6 mL) containing **PgFeTPP** (polymer catalyst, 10 mg, 13 μM of FeTPP unit), 1,3-dimethyl-2-phenyl-2,3-dihydro-1*H*-benzimidazole (BIH, electron doner; 50 mM) and IrBPY (photosensitizer, 0.1 mM) with an Xe light source ($\lambda >$ 400 nm). The amount of the porphyrin unit was calculated based on the feed amount of **FeTPP-M** in the polymerization step. After irradiation for 6 hours, **PgFeTPP-DVB10** with a particle size of 53–100 μm produced 4.9 μmol of CO and 0.20 μmol of H_2 (entry 4 in Table 2 and Fig. 7). The selectivity for CO production was 96%. The turnover number (TON) for CO was 37. In contrast, **PgTPP**, which contained no iron atoms, did not exhibit CO generation after 6 hours of light irradiation (entry 2 in Table 2). When the amount of
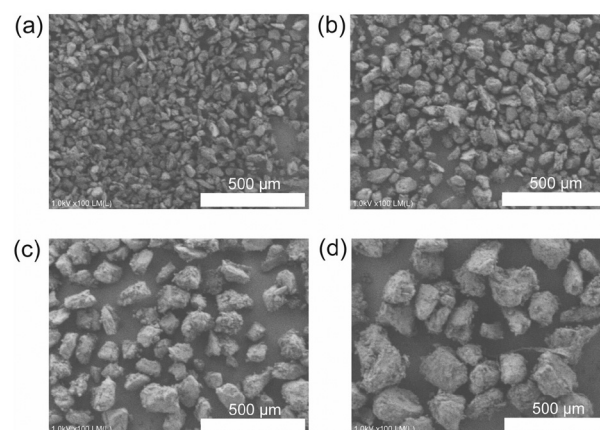

Fig. 6 SEM images of crushed **PgFeTPP-DVB10** particles classified using sieves. (a) ~53 μm, (b) 53–100 μm, (c) 100–150 μm, and (d) 150–250 μm.
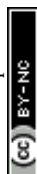
Table 2 Results of CO_2 photoreduction after 6 hours of visible light irradiation[a]

Entry	Catalyst	Particle size (μm)	CO (μmol)	H₂ (μmol)	Selectivity (CO%)	TON$_{CO}$	TOF$_{CO}$[b] (h⁻¹)
1[c]	**FeTPP**	—	10.3	0.75	95	79	24
2	**PgTPP**	53–100	0	0.20	—	—	—
3	**PgFeTPP-DVB10**	~53	4.89 ± 0.18	0.69 ± 0.12	88	38	8.5
4	**PgFeTPP-DVB10**	53–100	4.89 ± 0.04	0.24 ± 0.07	95	38	7.2
5	**PgFeTPP-DVB10**	100–150	5.37 ± 0.20	0.65 ± 0.17	89	41	8.2
6	**PgFeTPP-DVB10**	150–200	5.62 ± 0.67	0.34 ± 0.09	94	43	9.4
7	**PgFeTPP-DVB50**	53–100	1.30 ± 0.10	0.32 ± 0.15	80	10	1.8
8	**PgFeTPP-DVB100**	53–100	0.83 ± 0.06	0.23 ± 0.07	78	6.4	1.8

[a] A reaction solution was prepared by adding DMF (9.4 mL), PhOH (600 μL), IrBPY (0.1 mM), BIH (50 mM), and the catalyst. The concentration of FeTPP unit was 13 μM. The reaction started with irradiation of a white Xenon light ($\lambda > 400$ nm). [b] TOF$_{CO}$ was calculated using TON$_{CO}$ values after 1 and 2 hours of light irradiation (Tables S2 and S3†). [c] Small molecule of FeTPP was used.
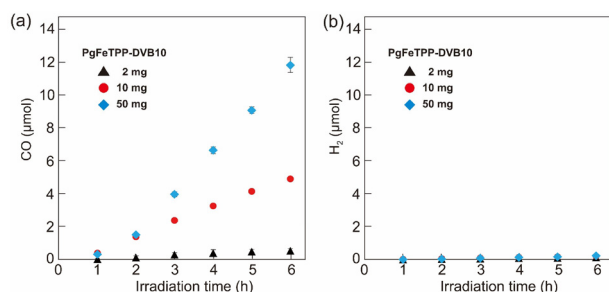
Fig. 7 Photocatalytic activity of **PgFeTPP-DVB10** at each dosage. Produced amount of carbon monoxide (a) and hydrogen (b). Black triangles (2 mg), red circles (10 mg), and blue diamonds (50 mg) represent the amount of **PgFeTPP-DVB10** in the reaction solution.

Fig. 8 (a) Photocatalytic activity of **PgFeTPP-DVB10** in each classified particle sizes. Black triangles (~53 μm), red circles (53–100 μm), blue diamonds (100–150 μm), and green squares (150–250 μm) represent the particle sizes. (b) Photocatalytic activity of **PgFeTPP-DVB10** with different cross-linking ratio. DVB feed ratios to total monomer amount are 10 (red circles), 50 (blue circles), and 100 wt% (orange circles), respectively.

PgFeTPP-DVB10 in the reaction solution was decreased (2 mg) or increased (50 mg), the amount of CO generated correspondingly changed (Fig. 7a). On the other hand, no correlation was observed between the amount of H₂ generated and the amount of polymer catalyst (Fig. 7b). These results confirm that the iron porphyrins incorporated into the polymer gels acted as the catalyst for the CO_2 reduction. Although the TON$_{CO}$ of **PgFeTPP-DVB10** was smaller than that of commercial iron porphyrin molecule (TON$_{CO}$ = 79, entry 1 in Table 2), a decrease in catalytic activity is a general tendency of heterogeneous catalysts. These results indicate that the synthesized polystyrene-based polymer gel incorporating FeTPP units functioned as a heterogeneous catalyst for CO_2 photoreduction.

Next, the effect of the particle sizes of the polymer gels were evaluated. After 6 hours of light irradiation, the CO production remained around 5.0 μmol for all particle sizes (entries 3–6 in Table 2 and Fig. 8a). The TON$_{CO}$ and TOF$_{CO}$ were also consistent across different particle sizes. Although a slight amount of H₂ was observed as a by-product (<0.82 μmol), the CO selectivity was consistently over 86% for all particle sizes. This indicates that the particle size, which corresponds to the surface area, did not impact CO_2 photoreduction in our system. If the catalytic reaction occurred solely on the particle surface, we would expect higher CO production from smaller particles due to their larger surface area. However, the lack of correlation between CO amount and particle size suggests that the cata-
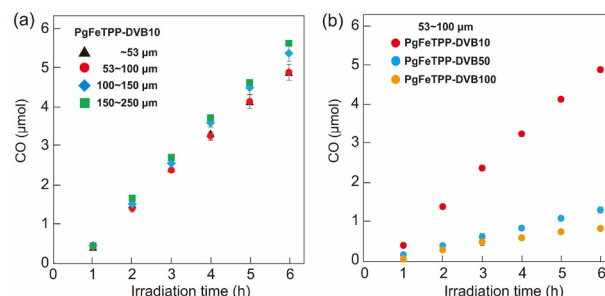
lytic reaction occurs not only on the particle surfaces but also within the particles.

For the catalytic reaction within the polymer gel particles, the substrate, and additives (CO_2, photosensitiser, proton donor, and electron donor) must diffuse into the polymer gel structures. To investigate the effect of cross-linking ratios of the polymer gels, we evaluated the photocatalytic reactivity of **PgFeTPP-DVB10**, **-DVB50**, and **-DVB100** (particle size: 53–100 μm). After 6 hours of light irradiation, **PgFeTPP-DVB10**, **-DVB50**, and **-DVB100** produced 4.9, 1.4, and 0.89 μmol of CO, respectively (entry 4, 7, and 8 in Table 2 and Fig. 8b). As the cross-linking ratio of **PgFeTPP** increased, CO generation tended to decrease. This decrease can be attributed to the suppressed diffusion of CO_2 or other additives into the more cross-linked polymer gel structures. These results highlight the unique property of polymer gel structures as scaffolds for heterogeneous photocatalysts, particularly in terms of internal substrate diffusion.

Conclusions

In this study, we prepared polystyrene-based polymer gels incorporating iron porphyrin (FeTPP) units and evaluated their

catalytic activity for CO_2 photoreduction. The polymer gels were synthesized by adjusting the feed ratio of the cross-linker (divinylbenzene). The successful incorporation of iron porphyrin units into the polymer structures were confirmed through diffuse reflectance UV-vis measurements and XRF analysis. The polymer gels containing FeTPP exhibited photocatalytic activity in converting CO_2 to CO under visible light irradiation. Interestingly, the particle sizes of the crushed polymer gels with the same cross-linking ratios did not correlate with the amount of CO produced. However, higher cross-linking ratio in the polymers led to a decreased in the amount of CO produced. These findings suggest that the observed reaction occurred within the polymer gel structures, facilitated by the internal diffusion of CO_2 and other additives. This work highlights the potential of polymer gels as effective scaffolds for heterogeneous catalysts in photoreactions and contributes to the development of practical and effective CO_2 photoreduction systems using principles of polymer chemistry.

Data availability

The data supporting this article have been included as part of the ESI.†

Conflicts of interest

There are no conflicts to declare.

Acknowledgements

References

1 A. Huovila, H. Siikavirta, C. A. Rozado, J. Rökman, P. Tuominen, S. Paiho, Å. Hedman and P. Ylén, *J. Cleaner Prod.*, 2022, **341**, 130912.

2 H. Rao, C.-H. Lim, J. Bonin, G. M. Miyake and M. Robert, *J. Am. Chem. Soc.*, 2018, **140**, 17830–17834.

3 Q. Huang, J. Liu, L. Feng, Q. Wang, W. Guan, L.-Z. Dong, L. Zhang, L.-K. Yan, Y.-Q. Lan and H.-C. Zhou, *Natl. Sci. Rev.*, 2020, **7**, 53–63.

4 S. Navarro-Jaén, M. Virginie, J. Bonin, M. Robert, R. Wojcieszak and A. Y. Khodakov, *Nat. Rev. Chem.*, 2021, **5**, 564–579.

5 C. Shen, X.-Y. Meng, R. Zou, K. Sun, Q. Wu, Y.-X. Pan and C.-J. Liu, *Angew. Chem., Int. Ed.*, 2024, e202402369.

6 T.-C. Zhuo, Y. Song, G.-L. Zhuang, L.-P. Chang, S. Yao, W. Zhang, Y. Wang, P. Wang, W. Lin, T.-B. Lu and Z.-M. Zhang, *J. Am. Chem. Soc.*, 2021, **143**, 6114–6122.

7 A. Nakada, K. Koike, T. Nakashima, T. Morimoto and O. Ishitani, *Inorg. Chem.*, 2015, **54**, 1800–1807.

8 C. Mesters, *Annu. Rev. Chem. Biomol. Eng.*, 2016, **7**, 223–238.

9 Y. Yamazaki, H. Takeda and O. Ishitani, *J. Photochem. Photobiol., C*, 2015, **25**, 106–137.

10 R. Bonetto, F. Crisanti and A. Sartorel, *ACS Omega*, 2020, **5**, 21309–21319.

11 R. Francke, B. Schille and M. Roemelt, *Chem. Rev.*, 2018, **118**, 4631–4701.

12 C. Costentin, M. Robert and J.-M. Savéant, *Chem. Soc. Rev.*, 2013, **42**, 2423–2436.

13 S. Zhang, Q. Fan, R. Xia and T. J. Meyer, *Acc. Chem. Res.*, 2020, **53**, 255–264.

14 C. Wang, Z. Sun, Y. Zheng and Y. H. Hu, *J. Mater. Chem. A*, 2019, **7**, 865–887.

15 L. Zou, R. Sa, H. Lv, H. Zhong and R. Wang, *ChemSusChem*, 2020, **13**, 6124–6140.

16 E. Boutin, L. Merakeb, B. Ma, B. Boudy, M. Wang, J. Bonin, E. Anxolabéhère-Mallart and M. Robert, *Chem. Soc. Rev.*, 2020, **49**, 5772–5809.

17 V. N. Gopalakrishnan, J. Becerra, E. F. Pena, M. Sakar, F. Béland and T.-O. Do, *Green Chem.*, 2021, **23**, 8332–8360.

18 E. Nikoloudakis, I. López-Duarte, G. Charalambidis, K. Ladomenou, M. Ince and A. G. Coutsolelos, *Chem. Soc. Rev.*, 2022, **51**, 6965–7045.

19 J. Bonin, M. Chaussemier, M. Robert and M. Routier, *ChemCatChem*, 2014, **6**, 3200–3207.

20 E. Pugliese, P. Gotico, I. Wehrung, B. Boitrel, A. Quaranta, M.-H. Ha-Thi, T. Pino, M. Sircoglou, W. Leibl, Z. Halime and A. Aukauloo, *Angew. Chem., Int. Ed.*, 2022, **61**, e202117530.

21 J. Jin, *New J. Chem.*, 2020, **44**, 15362–15368.

22 Z.-B. Fang, T.-T. Liu, J. Liu, S. Jin, X.-P. Wu, X.-Q. Gong, K. Wang, Q. Yin, T.-F. Liu, R. Cao and H.-C. Zhou, *J. Am. Chem. Soc.*, 2020, **142**, 12515–12523.

23 H. L. Nguyen and A. Alzamly, *ACS Catal.*, 2021, **11**, 9809–9824.

24 X. Ding, B. Yu, B. Han, H. Wang, T. Zheng, B. Chen, J. Wang, Z. Yu, T. Sun, X. Fu, D. Qi and J. Jiang, *ACS Appl. Mater. Interfaces*, 2022, **14**, 8048–8057.

25 P. L. Cheung, S. K. Lee and C. P. Kubiak, *Chem. Mater.*, 2019, **31**, 1908–1919.

26 A.-A. Zhang, D. Si, H. Huang, L. Xie, Z.-B. Fang, T.-F. Liu and R. Cao, *Angew. Chem., Int. Ed.*, 2022, **61**, e202203955.

27 Z. Dai, Q. Sun, X. Liu, C. Bian, Q. Wu, S. Pan, L. Wang, X. Meng, F. Deng and F.-S. Xiao, *J. Catal.*, 2016, **338**, 202–209.

28 J. Lu and P. H. Toy, *Chem. Rev.*, 2009, **109**, 815–838.

29 Q. Sun, Z. Dai, X. Meng and F.-S. Xiao, *Chem. Soc. Rev.*, 2015, **44**, 6018–6034.

30 M. Debruyne, V. V. Speybroeck, P. V. D. Voort and C. V. Stevens, *Green Chem.*, 2021, **23**, 7361–7434.

31 B. Altava, M. I. Burguete, E. García-Verdugo and S. V. Luis, *Chem. Soc. Rev.*, 2018, **47**, 2722–2771.

32 H. Matsumoto, T. Iwai, M. Sawamura and Y. Miura, *ChemPlusChem*, 2024, e202400039.

1030 | *RSC Appl. Polym.*, 2024, **2**, 1026–1031

© 2024 The Author(s). Published by the Royal Society of Chemistry

33 H. Matsumoto, H. Seto, T. Akiyoshi, M. Shibuya, Y. Hoshino and Y. Miura, *ACS Omega*, 2017, **2**, 8796–8802.

34 H. Matsumoto, Y. Hoshino, T. Iwai, M. Sawamura and Y. Miura, *ChemCatChem*, 2020, **12**, 4034–4037.

© 2024 The Author(s). Published by the Royal Society of Chemistry

RSC Appl. Polym., 2024, **2**, 1026–1031 | **1031**